Genomic footprints of activated telomere maintenance mechanisms in cancer

Lina Sieverling[1], Chen Hong[1], Sandra D. Koser[1], Philip Ginsbach[2], Kortine Kleinheinz[2], Barbara Hutter[1], Delia M. Braun[3], Isidro Cortés-Ciriano[4-6], Ruibin Xi[7], Rolf Kabbe[2], Peter J. Park[4,6], Roland Eils[2,8], Matthias Schlesner[2], Karsten Rippe[3], David T.W. Jones[9,10], Benedikt Brors[1,10], Lars Feuerbach[1], PCAWG-1, PCAWG-2, PCAWG-3, PCAWG-6, PCAWG-11, PCAWG-tech

[1]Division of Applied Bioinformatics, German Cancer Research Center (DKFZ), Heidelberg, Germany.

[2]Division of Theoretical Bioinformatics, German Cancer Research Center (DKFZ), Heidelberg, Germany.

[3]Research Group Genome Organization & Function, German Cancer Research Center (DKFZ) and BioQuant, Heidelberg, Germany.

[4]Department of Biomedical Informatics, Harvard Medical School, Boston, Massachusetts, USA.

[5]Centre for Molecular Science Informatics, Department of Chemistry, University of Cambridge, Cambridge, United Kingdom.

[6]Ludwig Center at Harvard, Boston, Massachusetts, USA.

[7]School of Mathematical Sciences and Center for Statistical Science, Peking University, Beijing, China.

[8]Department for Bioinformatics and Functional Genomics, Institute for Pharmacy and Molecular Biotechnology (IPMB) and BioQuant, Heidelberg, Germany.

[9]Division of Pediatric Neurooncology, German Cancer Research Center (DKFZ), Heidelberg, Germany.

[10]German Cancer Consortium (DKTK), Heidelberg, Germany.

Correspondence should be addressed to L.F. (l.feuerbach@dkfz-heidelberg.de)

Abstract

Unlimited replicative potential is a hallmark of cancer. It requires the maintenance of telomere repeats either by telomerase activation or by an alternative lengthening of telomeres (ALT) pathway. Here, we dissected whole-genome sequencing data of 2,519 matched tumor-control samples from 36 different tumor types to characterize the genomic footprints of these telomere maintenance mechanisms. While the telomere content of tumors with ALT-associated mutations was increased, tumors with putative telomerase activation showed a moderate decrease of telomere content. A systematic search discovered 2,683 somatic integrations of telomeric sequences into non-telomeric DNA. These telomere insertions were distributed across the genome and strongly correlated with increased telomere content, genomic breakpoint frequency and ALT-associated mutations. Moreover, ALT-associated mutations were significantly linked to telomere variant repeats, especially if embedded in canonical TTAGGG telomere repeats. This includes a previously undescribed accumulation of TTCGGG. Overall, our findings provide new insight into the recurrent genomic alterations that are associated with the establishment of different telomere maintenance mechanisms in tumors.

Telomeres are nucleoprotein complexes at the ends of chromosomes that prevent DNA degradation and genome instability[1]. The typically 10-15 kb long chromosome termini are composed of long stretches of TTAGGG (t-type) repeat arrays with an increasing number of variants towards proximal, subtelomeric regions, the most common being TGAGGG (g-type), TCAGGG (c-type) and TTGGGG (j-type) repeats[2,3].

Telomeres play an important role in cellular aging, as they are shortened with each cell division and finally trigger a DNA-damage response resulting in senescence[4,5]. To avoid this permanent growth arrest, cells with unlimited proliferative potential need to extend their telomeres. In humans, telomeric

DNA is synthesized onto the chromosome ends by telomerase, an enzyme that is composed of the reverse transcriptase TERT and the RNA template TERC and is active in the germline and stem cells, but absent in most somatic cells[6]. Telomerase is up-regulated in about 85% of human cancers by different mechanisms, including *TERT* amplifications[7], rearrangements[8-10] or mutations in the *TERT* promoter[11,12]. The remaining tumors employ an alternative lengthening of telomeres (ALT) pathway, which is based on DNA recombination of telomeric sequences[13]. Details on the ALT mechanism remain elusive but it has been associated with loss-of-function mutations in the chromatin remodeling genes *ATRX* (α-thalassaemia/mental retardation syndrome X-linked) and *DAXX* (death-domain associated protein)[14]. Telomeres of ALT cells characteristically have heterogeneous lengths and contain a range of telomere variant repeats (TVRs)[15-17]. Other hallmarks of ALT include ALT-associated promyelocytic leukemia (PML) nuclear bodies (APBs) and abundance of extrachromosomal telomeric repeats of various forms (such as C-circles)[13].

While normally located at the chromosome termini, telomere sequences are also found in intrachromosomal regions. As such, interstitial telomeric sequences with large blocks of telomere repeats exist in humans and other species, which probably arose from ancestral genome rearrangements or other evolutionary events[18]. Recently, ALT-specific, targeted telomere insertions into chromosomes that lead to genomic instability have also been described[19]. Another source for unexpected telomere repeat sites is the stabilizing function of telomeres at broken chromosomes. After a double-strand break, telomeres can be added *de novo* to the unprotected break sites ("telomere healing")[20,21] or acquired from other chromosomal positions ("telomere capture")[22,23].

Here, we characterized the telomere landscape of 2,519 tumor samples from 36 different tumor types using whole genome sequencing data. After searching for ALT-associated and putative telomerase-activating mutations, we focused on differences between these two sample subsets in terms of telomere content, tumor-specific telomere insertions and accumulation of TVRs. Our findings show significant increases in telomere content and number of telomere insertions in tumor samples with ALT-associated mutations. We further show that singleton TVRs in TTAGGG stretches are particularly informative about possible underlying telomere maintenance mechanisms (TMMs) and reveal previously uncharacterized TVRs specifically enriched in tumors with different TMM-associated mutations.

Results

Telomere content across cohorts

Due to the repetitive nature of telomere sequences, short sequencing reads from telomeres cannot be uniquely aligned to individual chromosomes. However, a mean telomere content can be estimated from the number of reads containing telomere sequences[17,24-27]. Here, we extracted reads containing at least six telomere repeats per 100 bases, allowing the canonical telomere repeat TTAGGG and the three most common TVRs TCAGGG, TGAGGG and TTGGGG. The telomere content was defined as the number of unaligned telomere reads normalized by sequencing coverage and GC-content. In this way, the telomere content of 2,519 tumor samples and matched controls from 36 different tumor types was determined.

Telomere content of the controls anti-correlated with age (r = -0.36, Spearman correlation) (Supplementary Fig. 1a). The strong correlation (r = 0.47, Spearman correlation) between the telomere content of the tumor and control samples is partially explained by this age effect (Supplementary Fig. 1b). We normalized for the correlation by computing the ratio of tumor to control telomere content.

Most tumor samples had a lower telomere content than the matched control (Fig. 1a). However, there were systematic differences between the different tumor types. Among those with the highest telomere content increase were osteosarcomas and leiomyosarcomas (median telomere content tumor/control log2 ratios = 0.7 and 0.3, respectively). A particularly low telomere content was found in colorectal adenocarcinoma and medulloblastoma (median telomere content tumor/control log2 ratios = -1.0).

Prevalence of TMM-associated mutations

Different types of mutations in *ATRX* or *DAXX* and around *TERT* have been associated with ALT and telomerase activation. We therefore searched for these types of somatic mutations to infer the active TMM. In total, 74 tumor samples had truncating *ATRX* (*n* = 63) or *DAXX* alterations (*n* = 11) and are referred to as ATRX/DAXX^{trunc} in the following. Of note, 10 of the 11 *DAXX* alterations were found in pancreatic endocrine tumors. An additional 46 samples had non-truncating *ATRX/DAXX* simple nucleotide variants. *TERT* alterations were detected in 256 tumor samples (TERT^{mod}). The latter group comprised 184 activating C228T or C250T promoter mutations, 12 amplifications leading to at least six additional *TERT* copies, 55 structural variations upstream of *TERT*, and 5 samples with several of these modifications. Additionally, 18 tumor samples had both *ATRX/DAXX* and *TERT* alterations.

The structural variations upstream of *TERT* were strikingly focal (Supplementary Fig. 2), suggesting an advantage of tumors with rearrangements near the *TERT* transcription start site (TSS). Moreover, 40% (*n* = 25/62) of the juxtaposed positions within 20 kb upstream of the *TERT* TSS overlapped directly with enhancers from the dbSUPER database[28]. In contrast, only 13% (n = 9/69) of the juxtaposed positions between 20 and 1,000 kb corresponded to a predicted super-enhancer. These results point to “enhancer hijacking” near the *TERT* TSS, a phenomenon which has been described in neuroblastoma[8,9] and for which indications have recently been found in further cancer types[29].

The tumor types with the highest prevalence of ATRX/DAXX^{trunc} mutations were adult lower grade gliomas (28%), leiomyosarcoma (24%), pancreatic endocrine tumors (23%) and osteosarcoma (17%) (Fig. 1b), all of which have previously been associated with ALT[14,30]. Importantly, the five lower grade

glioma samples with *ATRX* alterations are not oligodendrogliomas according to the recent WHO classification[31], as they are missing 1p/19q co-deletions. $TERT^{mod}$ were most prevalent in transitional cell bladder cancer (70%), glioblastoma (64%), lower grade gliomas (61%) and melanoma (46%).

The telomere content in $TERT^{mod}$ samples differed significantly from that in $ATRX/DAXX^{trunc}$ samples ($p = 2.4 \times 10^{-9}$, Wilcoxon rank-sum test; Fig. 1c, a detailed overview is shown in Supplementary Fig. 3a), but not from the telomere content in samples with non-truncating *ATRX/DAXX* simple nucleotide variants ($p > 0.05$, Wilcoxon rank-sum test). On average, telomere content was gained in $ATRX/DAXX^{trunc}$ (mean telomere content tumor/control log2 ratio = 0.2), while telomere sequences were lost in $TERT^{mod}$ samples (mean telomere content tumor/control log2 ratio = -0.4). In $TERT^{mod}$ samples and samples with unknown TMM, the telomere content correlated with *TERT* expression (r = 0.20, Pearson correlation; $p = 4.1 \times 10^{-10}$, significance of fitted linear regression model) and the *TERT* expression was significantly higher in $TERT^{mod}$ samples than in $ATRX/DAXX^{trunc}$ samples ($p = 1.2 \times 10^{-6}$, Wilcoxon rank-sum test; Fig. 1d, a detailed overview is shown in Supplementary Fig. 3b).

Telomere insertions occur frequently in tumors with ALT-associated mutations

To find insertions of telomeres into non-telomeric regions of the genome, we searched for tumor-specific discordant paired-end reads where one end maps to the chromosome and the other end is telomeric. Exact positions of the insertions were determined from reads spanning the junction site and visually inspected (examples in Fig. 2 and Supplementary Fig. 4).

Overall, 2,683 telomere insertions were detected. These were distributed unevenly between samples and different tumor types (Fig. 3a). While no telomere insertions were found in 73% of the tumor samples, the remaining samples had between one and 228 telomere insertion events. The tumor types with the highest amount of telomere insertions per tumor sample were leiomyosarcoma and osteosarcoma, both of which also had a relatively high mean telomere content. In fact, the number of telomere insertions positively correlated with the telomere content (r = 0.19, Spearman correlation). Moreover, the number of telomere insertions was associated with the number of genomic break points in the sample (r = 0.38, Spearman correlation). To test for a synergistic effect, linear models that predict telomere insertions from telomere content and breakpoint abundance with and without an interaction term were computed. The models with the interaction term ($p = 8.8 \times 10^{-234}$) performed substantially better than purely additive models ($p = 5.8 \times 10^{-90}$).

There was clearly a higher percentage of samples with telomere insertions in $ATRX/DAXX^{trunc}$ tumors (70%) than $TERT^{mod}$ tumors (29%) (Fig. 3b). As expected, $ATRX/DAXX^{trunc}$ samples also had a higher number of breakpoints (mean = 722) than $TERT^{mod}$ samples (mean = 298) (Fig. 3c). In keeping with this, chromothripsis (numerous chromosomal rearrangements occurring in a single event)[32] was more prevalent in the $ATRX/DAXX^{trunc}$ samples (59%) compared to $TERT^{mod}$ samples (34%) and samples without $ATRX/DAXX^{trunc}$ and $TERT^{mod}$ mutations (29%). Overall, the fraction of breakpoints overlapping with telomere insertion sites was significantly higher in $ATRX/DAXX^{trunc}$ than $TERT^{mod}$ samples ($p = 1.4 \times 10^{-15}$, Wilcoxon rank-sum test; Fig. 3d). Correlation analysis of telomere insertions and mutations in telomere maintenance-associated genes from the TelNet database (http://www.cancertelsys.org/telnet) revealed significant association with *TP53* ($q = 1.9 \times 10^{-42}$), *ATRX* ($q = 2.6 \times 10^{-6}$), *PLCB2* ($q = 7.8 \times 10^{-4}$), *MEN1* ($q = 0.017$), *TSSC4* ($q = 0.017$), *RB1* ($q = 0.018$),

DAXX (q = 0.019) and *ABCC8* mutations (q = 0.04, Wilcoxon rank-sum tests after Benjamini-Hochberg correction). Most of these genes have been implicated in the maintenance of telomere length or structure in humans (Supplementary Table 1). The exceptions are *PLCB2* and *ABCC8*, whose homologues have so far only been reported in association with telomere length regulation in yeast[33,34].

The detected telomere insertions were scattered across different chromosomes and regions within the chromosome (Supplementary Fig. 5). No clear preferential insertion sites were identified, but several *de novo* telomere junctions occurred at the chromosome ends (3% within 50 kb of the first or last chromosomal segment). A total of 44% of the telomere insertions were in genes, and 8% of these disrupted exons. Several tumor suppressor genes were affected, e.g. *CHEK1* encoding for a protein involved in cell cycle arrest upon DNA damage[35] (Fig. 2). This indicates that telomere insertions may directly contribute to tumor development.

Of note, patterns of microhomology were observed in 79% of telomere insertions with t-type repeats at the junction site (Supplementary Fig. 6).

Telomere insertions often coincide with loss of the adjacent chromosomal segment

Most of the telomere insertions were one-sided (98%), i.e. telomere sequences were only attached to one side of the breakpoint (example in Fig. 2). Telomere insertions were defined as two-sided if there was a second telomere insertion event downstream in the opposite orientation (example in Supplementary Fig. 4). Because so many breakpoints were one-sided, we investigated the fate of the corresponding broken fragment using complementary information from copy number changes and structural variation annotation. As expected, one-sided telomere insertions coincided most frequently with copy number loss of the adjacent segment (46%) (Fig. 3e). In contrast, copy number gains of the fragment were rare (6%). Surprisingly, telomere insertions were frequently located at copy number neutral sites (43%). Overlaps with regions of chromothripsis were found for 24% and structural variations without chromothripsis overlap (including telomere insertions) were detected near the insertion site for 28% of the copy-number neutral cases.

Singleton TVRs are enriched in ATRX/DAXX^{trunc} samples

It has previously been shown that ALT leads to an increased integration of TVRs into telomeres, the most common ones being hexamers of the type NNNGGG[17]. To detect differences in the telomere composition of ATRX/DAXX^{trunc} and TERT^{mod} tumors, we therefore searched for NNNGGG repeats in telomere reads. The most frequent TVRs across all tumor samples were TGAGGG, TCAGGG and TTGGGG (Supplementary Fig. 7), which are known to be enriched in proximal telomeric regions [2,3].

These and the seven other most frequent TVRs (TAAGGG, GTAGGG, CATGGG, TTCGGG, CTAGGG, TTTGGG and ATAGGG) were chosen to search for common telomere repeat combinations. For this, the neighboring 18 base pairs on either side of the TVRs were determined (Supplementary Table 2). Most TVRs were surrounded by many different pattern combinations (e.g. TTGGGG). Others were dominated by a certain repeat context, which was similar in ATRX/DAXX^{trunc} and TERT^{mod} tumors (e.g. CATGGG or ATAGGG). However, TTCGGG stood out, as 33% of the TVRs in ATRX/DAXX^{trunc} samples were surrounded by canonical t-type repeats, whereas this context was observed in only 2% of TTCGGG TVRs in TERT^{mod} tumors.

Comparison of variant hexamers surrounded by t-type repeats ("singletons") to TVRs in an arbitrary sequence context further revealed that the former are generally better suited to distinguish ALT-positive from telomerase-positive samples (Supplementary Fig. 8). The remaining variant analysis therefore focused on singleton repeats. CATGGG was excluded as it did not occur as singleton repeats. For the other TVRs, the median of absolute counts varied between 13 and 112, but counts in individual tumor samples reached more than ten thousand (Supplementary Fig. 9).

As expected, normalized singleton repeat counts generally rose with increasing telomere content (Fig. 4a, an overview of all patterns is shown in Supplementary Fig. 10). However, TGAGGG, TCAGGG, TTGGGG and TTCGGG singleton repeats had significantly higher counts than expected in ATRX/DAXX^{trunc} compared to TERT^{mod} samples ($p = 9.3 \times 10^{-7}$, 8.8×10^{-5}, 1.7×10^{-3}, and 1.8×10^{-9}, respectively, Wilcoxon rank sum test after Bonferroni correction; Fig. 4b). Especially TGAGGG and TTCGGG seemed to be highly interspersed in a subset of ATRX/DAXX^{trunc} tumors. In contrast, TTTGGG singleton repeats were observed less frequently in ATRX/DAXX^{trunc} tumors ($p = 3.5 \times 10^{-9}$, Wilcoxon rank sum test after Bonferroni correction).

This seemingly ALT-specific TVR enrichment or depletion occurred in different tumor types, with the highest prevalence in pancreatic endocrine tumors (42%), leiomyosarcoma (41%), lower grade gliomas and osteosarcomas (both 28%) (Supplementary Table 3, Supplementary Fig. 11). In the ATRX/DAXX^{trunc} samples, singleton TVR occurrences correlated (Supplementary Fig. 12). The strongest correlations were between TTCGGG enrichment and TGAGGG occurrence (r = 0.63, Pearson correlation) and TTTGGG depletion (r = -0.58, Pearson correlation).

ALT prediction

ALT has several different hallmarks with which it can be reliably identified[13]. However, none of these are detectable in short-read whole-genome sequencing data. Using ATRX/DAXX^{trunc} alterations as indicators for ALT, we have shown characteristics of ALT-associated samples in terms of telomere content, rearrangements and composition. Detailed information for all samples is provided in Supplementary Table 4. The following eight features were selected to further distinguish ALT-positive from telomerase-positive samples: telomere content tumor/control log2 ratio, number of telomere insertions, number of breakpoints and the divergence of observed TGAGGG, TCAGGG, TTGGGG, TTCGGG and TTTGGG singleton repeat counts from their expected occurrence.

A principal component analysis with the selected features discriminated ATRX/DAXX^{trunc} from TERT^{mod} samples. More than 75% of variances were contained in the first four principal components (Supplementary Fig. 13), showing that the selected features are well suited to separate samples by their putative TMM. The features were then used to build a random forest classifier based on the same grouping (area under the curve: 0.93; sensitivity: 0.66; specificity: 0.98; all after 10-fold cross-validation). The variables with the highest importance for the classification were the number of breakpoints and the divergence of observed TTCGGG and TTTGGG singleton TVRs to the expected count (Supplementary Table 5). The scores resulting from the classifier can be interpreted as an ALT probability. As expected, ATRX/DAXX^{trunc} had a high ALT probability (mean = 0.90), while TERT^{mod} samples had a low ALT probability (mean = 0.15, Supplementary Fig. 14). A total of 15 samples without ATRX/DAXX^{trunc} mutations had a ALT probability of over 0.9, of which two had non-truncating ATRX/DAXX mutations

and one sample had a truncating mutation in *ATRX* and a *TERT* amplification. Across the entire dataset, most samples had a low ALT probability (Fig. 5), suggesting that their TMM is telomerase-based. This included some samples with ATRX/DAXX missense mutations, suggesting that the mutations in those samples may be more of a passenger event than functionally relevant. Tumor types with a high ALT-probability were leiomyosarcoma, osteosarcoma and pancreatic endocrine tumors, in keeping with the known high prevalence of ALT in these entities[36,37].

Discussion

In this study, we have shown that the presence of ALT-associated mutations in tumors correlates with increased telomere content, enrichment of isolated TVRs in t-type context (singletons), a higher number of genomic breakpoints and intrachromosomal telomere insertions (Fig. 6). In contrast, tumors with mutations associated with a possible telomerase-activation showed moderate decrease of telomere content and increased *TERT* expression. The observed telomere content increase in ALT-associated versus the decrease in telomerase-associated samples is in agreement with the recent findings of Barthel *et al.*[29]. The higher telomere content in ALT-positive tumors could indicate that the negative feedback loop that constrains telomere elongation to a physiological level in healthy telomerase-expressing cells[38,39] is bypassed by the ALT process, while it seems to remain intact in telomerase-positive tumors. In contrast, ALT-positive tumors are subject to a less regulated process, which circumvents negative feedback regulation. In addition to telomere elongation, the increase of telomere content in ALT-positive tumors detected by sequencing-based methods may partly stem from aberrant intra-chromosomal telomere insertions[19] or extra-chromosomal telomeric DNA[40].

In our study, we systematically mapped telomere insertions into non-telomeric genomic regions using whole-genome sequencing data. They were most frequently accompanied by a loss of the adjacent chromosomal segment or located at copy number neutral sites. Surprisingly, the latter telomere insertions were rarely two-sided and chromothripsis or other structural variations in the adjacent genomic regions occurred only in about half of the cases. Whether the remaining segments have subclonal copy number changes or undetected structural variations is unclear. Taken together, the results suggest that we observe telomere healing or capture[21,22] rather than telomere insertions followed by chromosomal instabilities[19,41]. As microhomology around telomere insertion sites was frequent, the sequences were probably inserted by nonhomologous end-joining[42] or a microhomology-mediated mechanism[43].

Telomere insertions were particularly frequent in ATRX/DAXX^{trunc} tumors, in which the abundant extra-chromosomal telomeric DNA expands the telomere template pool for microhomology-mediated double strand repair. We speculate that in this cellular environment, a high load of genomic breakpoints subsequently leads to the observed disproportionately increased number of telomere capture-like events. Due to the stochastic nature of ALT, the likelihood of telomere crisis is elevated. The recently described induction of chromothripsis by telomere crisis[44] may thus explain the observed higher prevalence of chromothripsis in ATRX/DAXX^{trunc} cases in this study.

Telomere elongation by ALT or telomerase enriches distinct TVRs[17]. Here, we report a stronger association of singleton TVRs with ATRX/DAXX^{trunc} mutations than TVRs in an arbitrary context. The increase of TVRs has been attributed to the inclusion of subtelomeric regions during ALT via homologous recombination[16]. Whether telomeric sequences with lower TVR density are under positive selection or regions with higher TVR density are under negative selection remains to be clarified.

Enrichment of TCAGGG repeats that recruit nuclear receptors has been reported in ALT-positive cell lines[16,19]. This enrichment was confirmed in primary ATRX/DAXX^{trunc} tumor samples in our study, but was not as strong as the enrichment of TTCGGG or TGAGGG. Notably, only TTTGGG singletons were frequently depleted in ATRX/DAXX^{trunc} samples. The strong enrichment of TTCGGG singletons has not

been described previously to this extent and functional studies are needed to reveal potential roles of this TVR in ALT. For example, TVRs may drive deprotection of telomeres by disrupting binding of the shelterin complex, and/or may alter the telomeric G-quadruplex conformation.

The here presented methodologies expand the established telomere content estimation from genomic sequencing by the analysis of TVRs and telomere insertions, thus adding new dimensions for the characterization of different telomere maintenance mechanisms.

References

1. O'Sullivan, R.J. & Karlseder, J. Telomeres: protecting chromosomes against genome instability. *Nat Rev Mol Cell Biol* **11**, 171-81 (2010).
2. Allshire, R.C., Dempster, M. & Hastie, N.D. Human telomeres contain at least three types of G-rich repeat distributed non-randomly. *Nucleic Acids Res* **17**, 4611-27 (1989).
3. Baird, D.M., Jeffreys, A.J. & Royle, N.J. Mechanisms underlying telomere repeat turnover, revealed by hypervariable variant repeat distribution patterns in the human Xp/Yp telomere. *EMBO J* **14**, 5433-43 (1995).
4. Harley, C.B., Futcher, A.B. & Greider, C.W. Telomeres shorten during ageing of human fibroblasts. *Nature* **345**, 458-60 (1990).
5. d'Adda di Fagagna, F. *et al.* A DNA damage checkpoint response in telomere-initiated senescence. *Nature* **426**, 194-8 (2003).
6. Wright, W.E., Piatyszek, M.A., Rainey, W.E., Byrd, W. & Shay, J.W. Telomerase activity in human germline and embryonic tissues and cells. *Dev Genet* **18**, 173-9 (1996).
7. Zhang, A. *et al.* Frequent amplification of the telomerase reverse transcriptase gene in human tumors. *Cancer Res* **60**, 6230-5 (2000).
8. Peifer, M. *et al.* Telomerase activation by genomic rearrangements in high-risk neuroblastoma. *Nature* **526**, 700-4 (2015).
9. Valentijn, L.J. *et al.* TERT rearrangements are frequent in neuroblastoma and identify aggressive tumors. *Nat Genet* **47**, 1411-4 (2015).
10. Karlsson, J. *et al.* Activation of human telomerase reverse transcriptase through gene fusion in clear cell sarcoma of the kidney. *Cancer Lett* **357**, 498-501 (2015).
11. Horn, S. *et al.* TERT promoter mutations in familial and sporadic melanoma. *Science* **339**, 959-61 (2013).
12. Huang, F.W. *et al.* Highly recurrent TERT promoter mutations in human melanoma. *Science* **339**, 957-9 (2013).
13. Cesare, A.J. & Reddel, R.R. Alternative lengthening of telomeres: models, mechanisms and implications. *Nat Rev Genet* **11**, 319-30 (2010).
14. Heaphy, C.M. *et al.* Altered telomeres in tumors with ATRX and DAXX mutations. *Science* **333**, 425 (2011).
15. Varley, H., Pickett, H.A., Foxon, J.L., Reddel, R.R. & Royle, N.J. Molecular characterization of inter-telomere and intra-telomere mutations in human ALT cells. *Nat Genet* **30**, 301-5 (2002).
16. Conomos, D. *et al.* Variant repeats are interspersed throughout the telomeres and recruit nuclear receptors in ALT cells. *J Cell Biol* **199**, 893-906 (2012).
17. Lee, M. *et al.* Telomere extension by telomerase and ALT generates variant repeats by mechanistically distinct processes. *Nucleic Acids Res* **42**, 1733-46 (2014).
18. Lin, K.W. & Yan, J. Endings in the middle: current knowledge of interstitial telomeric sequences. *Mutat Res* **658**, 95-110 (2008).
19. Marzec, P. *et al.* Nuclear-receptor-mediated telomere insertion leads to genome instability in ALT cancers. *Cell* **160**, 913-27 (2015).
20. Wilkie, A.O., Lamb, J., Harris, P.C., Finney, R.D. & Higgs, D.R. A truncated human chromosome 16 associated with alpha thalassaemia is stabilized by addition of telomeric repeat (TTAGGG)n. *Nature* **346**, 868-71 (1990).
21. Flint, J. *et al.* Healing of broken human chromosomes by the addition of telomeric repeats. *Am J Hum Genet* **55**, 505-12 (1994).
22. Meltzer, P.S., Guan, X.Y. & Trent, J.M. Telomere capture stabilizes chromosome breakage. *Nat Genet* **4**, 252-5 (1993).
23. Slijepcevic, P. & Bryant, P.E. Chromosome healing, telomere capture and mechanisms of radiation-induced chromosome breakage. *Int J Radiat Biol* **73**, 1-13 (1998).
24. Parker, M. *et al.* Assessing telomeric DNA content in pediatric cancers using whole-genome sequencing data. *Genome Biol* **13**, R113 (2012).
25. Ding, Z. *et al.* Estimating telomere length from whole genome sequence data. *Nucleic Acids Res* **42**, e75 (2014).
26. Nersisyan, L. & Arakelyan, A. Computel: computation of mean telomere length from whole-genome next-generation sequencing data. *PLoS One* **10**, e0125201 (2015).
27. Lee, M. *et al.* Comparative analysis of whole genome sequencing-based telomere length measurement techniques. *Methods* **114**, 4-15 (2017).
28. Khan, A. & Zhang, X. dbSUPER: a database of super-enhancers in mouse and human genome. *Nucleic Acids Res* **44**, D164-71 (2016).
29. Barthel, F.P. *et al.* Systematic analysis of telomere length and somatic alterations in 31 cancer types. *Nat Genet* (2017).

30. Heaphy, C.M. *et al.* Prevalence of the alternative lengthening of telomeres telomere maintenance mechanism in human cancer subtypes. *Am J Pathol* **179**, 1608-15 (2011).
31. Louis, D.N. *et al.* The 2016 World Health Organization Classification of Tumors of the Central Nervous System: a summary. *Acta Neuropathol* **131**, 803-20 (2016).
32. Stephens, P.J. *et al.* Massive genomic rearrangement acquired in a single catastrophic event during cancer development. *Cell* **144**, 27-40 (2011).
33. Hu, Y. *et al.* Telomerase-null survivor screening identifies novel telomere recombination regulators. *PLoS Genet* **9**, e1003208 (2013).
34. Askree, S.H. *et al.* A genome-wide screen for Saccharomyces cerevisiae deletion mutants that affect telomere length. *Proc Natl Acad Sci U S A* **101**, 8658-63 (2004).
35. Patil, M., Pabla, N. & Dong, Z. Checkpoint kinase 1 in DNA damage response and cell cycle regulation. *Cell Mol Life Sci* **70**, 4009-21 (2013).
36. Amorim, J.P., Santos, G., Vinagre, J. & Soares, P. The Role of ATRX in the Alternative Lengthening of Telomeres (ALT) Phenotype. *Genes (Basel)* **7**(2016).
37. de Wilde, R.F. *et al.* Loss of ATRX or DAXX expression and concomitant acquisition of the alternative lengthening of telomeres phenotype are late events in a small subset of MEN-1 syndrome pancreatic neuroendocrine tumors. *Mod Pathol* **25**, 1033-9 (2012).
38. van Steensel, B. & de Lange, T. Control of telomere length by the human telomeric protein TRF1. *Nature* **385**, 740-3 (1997).
39. Hockemeyer, D. & Collins, K. Control of telomerase action at human telomeres. *Nat Struct Mol Biol* **22**, 848-52 (2015).
40. Nabetani, A. & Ishikawa, F. Unusual telomeric DNAs in human telomerase-negative immortalized cells. *Mol Cell Biol* **29**, 703-13 (2009).
41. Jia, P., Chastain, M., Zou, Y., Her, C. & Chai, W. Human MLH1 suppresses the insertion of telomeric sequences at intra-chromosomal sites in telomerase-expressing cells. *Nucleic Acids Res* (2016).
42. Lieber, M.R. The mechanism of double-strand DNA break repair by the nonhomologous DNA end-joining pathway. *Annu Rev Biochem* **79**, 181-211 (2010).
43. Ottaviani, D., LeCain, M. & Sheer, D. The role of microhomology in genomic structural variation. *Trends Genet* **30**, 85-94 (2014).
44. Maciejowski, J., Li, Y., Bosco, N., Campbell, P.J. & de Lange, T. Chromothripsis and Kataegis Induced by Telomere Crisis. *Cell* **163**, 1641-54 (2015).
45. Feuerbach, L. *et al.* TelomereHunter: telomere content estimation and characterization from whole genome sequencing data. *bioRxiv* (2016).
46. Robinson, J.T. *et al.* Integrative genomics viewer. *Nat Biotechnol* **29**, 24-6 (2011).
47. Thorvaldsdottir, H., Robinson, J.T. & Mesirov, J.P. Integrative Genomics Viewer (IGV): high-performance genomics data visualization and exploration. *Brief Bioinform* **14**, 178-92 (2013).
48. Korbel, J.O. & Campbell, P.J. Criteria for inference of chromothripsis in cancer genomes. *Cell* **152**, 1226-36 (2013).
49. Harrow, J. *et al.* GENCODE: the reference human genome annotation for The ENCODE Project. *Genome Res* **22**, 1760-74 (2012).
50. Liaw, A.W., M. Classification and Regression by randomForest. *R News* **2**, 18-22 (2002).
51. Kuhn, M. Building Predictive Models in R Using the caret Package. *Journal of Statistical Software; Vol 1, Issue 5 (2008)* (2008).

Methods

Sequencing data.

Whole genome sequencing (WGS) and expression data were obtained from the PanCancer Analysis of Whole Genomes (PCAWG) project (REF to PanCancer marker paper when available). The WGS reads of tumor and control samples were aligned with bwa-mem by the PCAWG-tech group. Tumors with multiple samples were excluded from this study, as well as a sample pair with reads shorter than 30 bp. Expression data was in the format of normalized RNA read counts per gene and only available for 1033 of 2,519 patients. Of note, we used the name "CNS-LGG" for the "CNS-Oligo" tumor type, because several samples in this cohort did not have the genetic markers for oligodendroglioma required by the WHO[31].

Mutation data.

Somatic simple nucleotide, structural variations and copy numbers were obtained from the PCAWG consensus calls (REF when available). Structural variations were not available for 24 tumor samples.

Telomere read extraction and computational telomere content estimation.

The telomere content of WGS samples was determined using the software tool TelomereHunter (www.dkfz.de/en/applied-bioinformatics/telomerehunter/telomerehunter.html)[45]. In short, telomeric reads containing six non-consecutive instances of the four most common telomeric repeat types (TTAGGG, TCAGGG, TGAGGG and TTGGGG) were extracted. For the further analysis, only unmapped reads or reads with a very low alignment confidence (mapping quality lower than 8) were considered. The telomere content was determined by normalizing the telomere read count by all reads in the sample with a GC-content of 48-52%.

Determining TMM-associated mutations.

Samples with a truncating *ATRX* or *DAXX* alteration (frame-shift insertion/deletion, stop-codon gain or structural variation breakpoint within the gene) were defined as ATRX/DAXX^{trunc}, samples with other simple nucleotide variants were defined as ATRX/DAXX$^{non\text{-}trunc}$. Samples with a structural variation breakpoint on the plus strand 20 kb upstream of *TERT* the transcription start site were defined as TERTp^{SV}. TERT^{amp} samples had at least six additional copies of the *TERT* gene compared to the mean ploidy of the sample. Tumor samples with a C228T or C250T *TERT* promoter mutation were defined as TERTp^{mut}. Due to the low sequencing coverage at the *TERT* promoter, these mutations were called using less stringent criteria (at least two reads with the mutated base, mutational frequency of at least 20%). If multiple of these *TERT* modifications were present, the sample was defined as TERT^{mult}. Samples with these *TERT* alterations were summarized as TERT^{mod}. Samples without any of these alterations were defined as "Other". If a sample had both a TERT^{mod} alteration and an *ATRX/DAXX* alteration, it was defined as "Mixed" for detailed analysis or included in "Other" for summary analysis.

Overlap of juxtaposed positions upstream of *TERT* and predicted super-enhancers.

For the closest structural variation (SV) of each tumor sample to the *TERT* TSS, the juxtaposed genomic coordinates were compared to 65,950 predicted super-enhancers from the dbSUPER database[28]. Only SVs on the plus strand and within 1 mb of the *TERT* TSS were considered. Overlaps of juxtaposed positions with super-enhancer sites were defined as direct overlaps. Super-enhancer sites within 1 mb of the juxtaposed position were defined as indirect overlaps.

Telomere insertion detection.

To find insertions of telomeric sequences into non-telomeric regions in the genome, we searched for tumor-specific discordant paired-end reads, where one end was an extracted telomere read and the other end was non-telomeric and uniquely mapped to a chromosome (mapping quality > 30). In 1 kb regions containing at least three discordant reads in the tumor sample and none in the matching control, exact positions of telomere insertions were defined by at least three split reads spanning the insertion site. The split reads had to contain at least one TTAGGG repeat. Regions with discordant read pairs in at least 15 control samples were excluded. Finally, the insertion sites were visualized using the Integrative Genomics Viewer (IGV)[46,47] to identify and remove remaining false positives. A telomere insertion was defined as two-sided if another telomere insertion in opposite orientation was found in the downstream 10 kb of the reference genome. Otherwise it was defined as one-sided.

Breakpoint detection.

Breakpoints were obtained from the consensus breakpoint list of structural and copy number variation calls. In short, six copy number detection tools were run on all samples including the consensus structural variations breakpoints. From the obtained chromosomal segments of the individual callers another set of consensus breakpoints was calculated (REF to CNV working group when available).

Chromothripsis detection.

To identify chromothripsis events, we extended the set of statistical criteria proposed by Korbel and Campbell[48]. The basic idea is to determine whether there is a statistically significant number of interleaved structural variants (SVs) in a contiguous genomic region. We did this by constructing a graph whose nodes correspond to SVs and whose edges connect interleaved SVs. The identified clusters of SVs were also tested for the presence of alternating copy number and loss-of-heterozygosity patterns. The resulting chromothripsis calls were validated visually. The full description of the methodology and the detailed patterns of chromothripsis events in the genomes will be reported in a separate manuscript by Cortes-Ciriano *et al.* [PCAWG 2017, Cortés-Ciriano *et al.*: Chromothripsis-like patterns are pervasive in human cancers]. Only high-confidence chromothripsis calls were included in this analysis.

Copy number changes at telomere insertion sites.

Copy numbers of chromosomal segments were obtained from the PCAWG consensus calls (REF when available). Copy numbers reveal gains or losses of chromosomal segments based on coverage and B-allele frequency, but were here limited to segments of at least 10 kb. The breakpoint estimations could differ from the actual site by up to 50 kb. Therefore, telomere insertions were assigned to the closest

breakpoint within 50 kb. If there was no breakpoint within 50 kb or the copy numbers at either side of the telomere insertion were the same, the copy number change at the telomere insertion was defined as neutral.

Structural variations near telomere insertion sites.

Structural variation annotation was obtained from the PCAWG consensus calls (REF when available), which was based on discordant mate pairs and split reads, providing exact breakpoints. Because copy number variations smaller than 10 kb were not detected by copy number callers, small deletions next to the telomere insertion site may be missed. We therefore searched for structural variations within 10 kb of a telomere insertion to detect these cases.

Candidate gene selection for correlation analysis.

A list of 1,725 telomere maintenance associated human genes was obtained from TelNet (http://www.cancertelsys.org/telnet/, REF to TelNet paper when available) on February 20 2017. After removing genes without a unique Ensembl IDs in the GENCODE[49] v19 HAVANA annotation, the remaining 1,686 genes were used for correlation of telomere insertions and simple nucleotide variants.

Detection of telomere repeat variants.

Telomere repeat variants (TVRs) were detected by searching for hexamers of the type NNNGGG in the extracted telomere reads. Each base was required to have a base quality of at least 20. The neighboring 18 bp on either side of the TVR were determined. For further analysis, NNNGGG TVRs were once computed for arbitrary context and once for t-type context ($(TTAGGG)_3$-NNNGGG-$(TTAGGG)_3$, also called “singletons”). The absolute counts were normalized to the total number of reads in the sample. The expected pattern counts at different telomere content tumor/control log2 ratios were taken from the regression line through telomerase-positive samples.

Principal component analysis (PCA).

Eight features were selected for the PCA: telomere content tumor/control log2 ratio, number of telomere insertions, number of break points and the distance of TGAGGG, TCAGGG, TTGGGG, TTCGGG and TTTGGG singleton repeats (i.e. repeats in a t-type context) to their expected occurrence. The PCA was performed on the selected features of the ATRX/DAXX^{trunc} and TERT^{mod} tumor samples. Three samples were excluded due to missing data, leaving 327 samples for the analysis.

Classifier for predicting active telomere maintenance mechanisms.

A random forest classifier to distinguish ATRX/DAXX^{trunc} and TERT^{mod} samples was built using the R packages “randomForest”[50] and “caret”[51] with the same features as for the PCA. To deal with the imbalance in the data set (i.e. 254 TERT^{mod} samples vs. 73 ATRX/DAXX^{trunc} samples without missing data), the model was trained with a down-sampled training set. The performance was determined using 10-fold cross-validation.

Statistics.

Differences between ATRX/DAXX^{trunc} and TERT^{mod} samples in terms of telomere content, percent break points with telomere insertions and singleton repeat abundance were tested using two-sided Wilcoxon rank-sum tests. Singleton repeat abundance p-values were corrected for multiple testing using the Bonferroni method. To reduce the influence of outliers, correlation coefficients were calculated with the Spearman method. Correlation between control telomere content and age as well as tumor and control telomere content was tested with linear regression. All statistical analyses were carried out using R (R Foundation for Statistical Computing).

Acknowledgments

We thank all PCAWG groups that have provided mutation calls. We thank J. Kerssemakers, M. Prinz and M. Heinold for their help in data processing. We thank I. Buchhalter for annotation of simple nucleotide variations. We thank D. Hübschmann for his support in correlation analysis. We thank all TelNet curators for sharing the results of their extensive literature research. We thank K.I. Deeg, P. Lichter, and S.M. Pfister for their support in early stages of the study. We thank I. Chung for comments and discussion. The work was supported by grants from the German Federal Ministry of Education and Research (BMBF) within the e:Med program (project CancerTelSys, 01ZX1302 to K.R.) and the program for medical genome research (01KU1001A, -B, -C, and -D; 01KU1505A). S.D.K. received funding from the German Research Foundation (DFG) in research priority program SPP1463 (grant no. Br3535/1-2). I.C.C. has received funding from the European Union's Framework Programme For Research and Innovation Horizon 2020 (2014-2020) under the Marie Sklodowska-Curie Grant Agreement No. 703543.

Author Contributions

L.S. was involved in all bioinformatical analyses. C.H. performed structural variation annotation, principal component analysis and classification. L.F. was responsible for correlation analysis. S.D.K. analyzed gene expression data and was involved in visualization. L.S., P.G. and L.F. were involved in method development. K.K. and M.S. were involved in copy number analysis. R.K. was involved in data pre-processing. D.M.B. developed and curated the TelNet database. I.C.C., R.X. and P.J.P. provided regions of chromothripsis. B.H. was involved in early stages of experimental design. R.E. was responsible for data management and creating the IT-infrastructure. K.R. and D.T.W.J. provided insights into telomere biology. D.T.W.J. and L.F. conceived the study. B.B. and L.F. oversaw the experimental design and execution. L.S. and L.F. wrote the manuscript with contributions by K.K., D.M.B., M.S., K.R. and D.T.W.J.

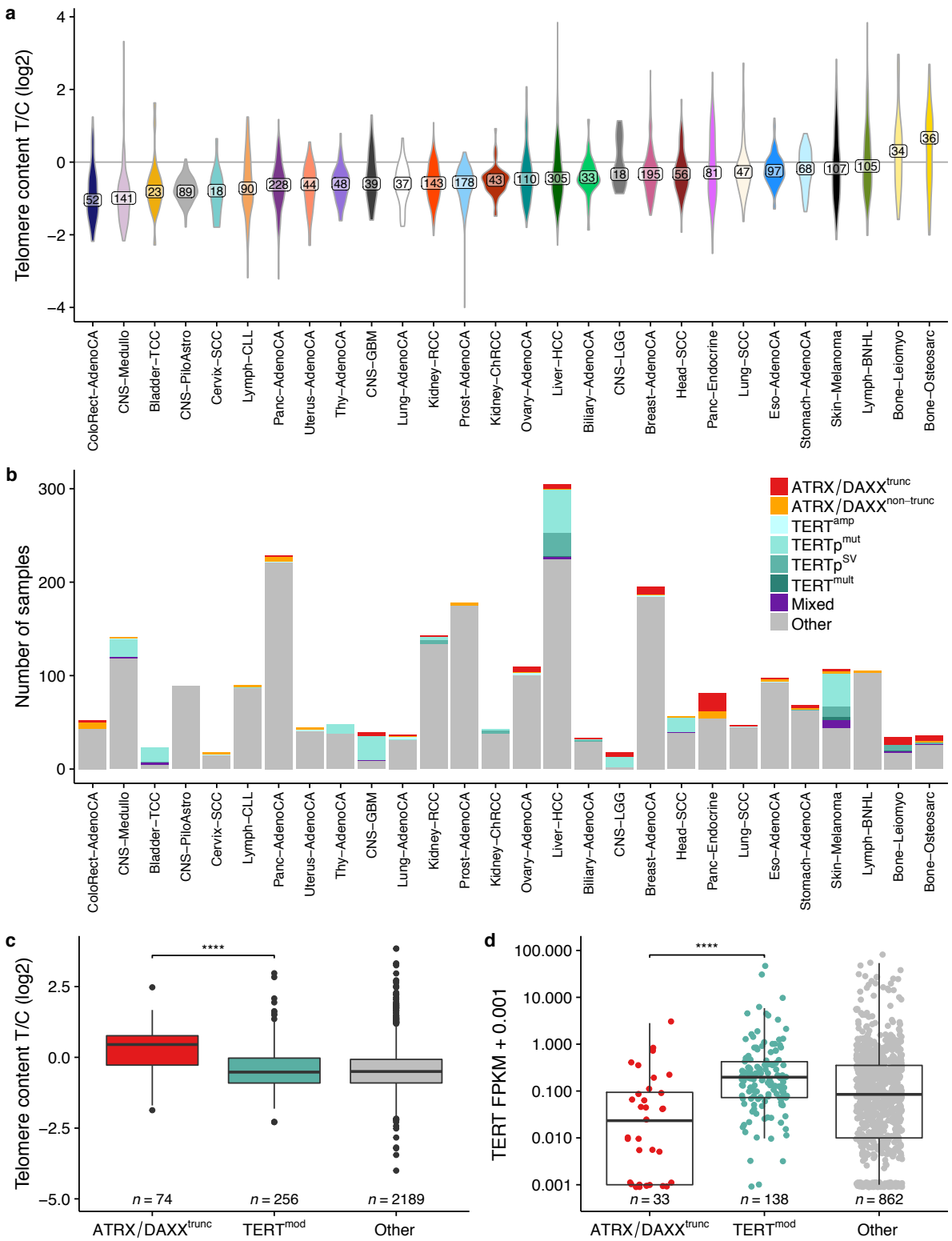

Figure 1: Telomere content is increased in ATRX/DAXX^{trunc} samples. (a) Overview of the telomere content distribution of all analyzed tumor types. The number of samples in each tumor type is indicated. Cohorts with sample sizes below 15 are not shown. (b) TMM-associated mutations in different tumor types. (c) Telomere content in samples with different TMM-associated mutations. (d) *TERT* expression in samples with different TMM-associated mutations. ****$p < 0.0001$, Wilcoxon rank-sum tests.

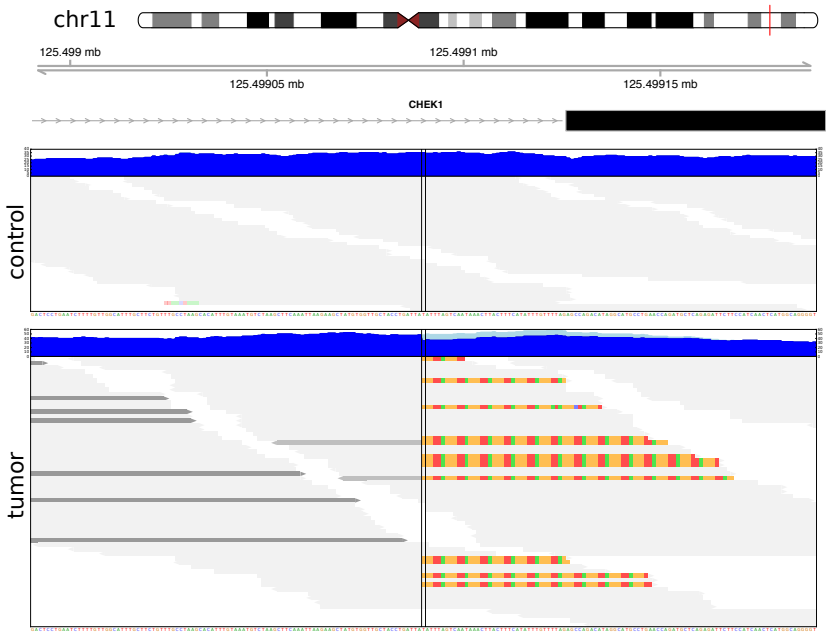

Figure 2: Example of reads mapping to a one-sided telomere insertion in leiomyosarcoma sample 854e42bc-95b2-4b77-a4b2-ffbd6c28b281. Telomere repeats are inserted into the gene *CHEK1* in the tumor sample, but not in the matching control. Blue tracks show the sequencing coverage at the position, light blue represents clipped sequences. Clipped bases are colored and telomeric repeats are opaque. Dark grey reads represent the non-telomeric end of a discordant read pair, medium grey reads represent the telomeric end of a discordant read pair.

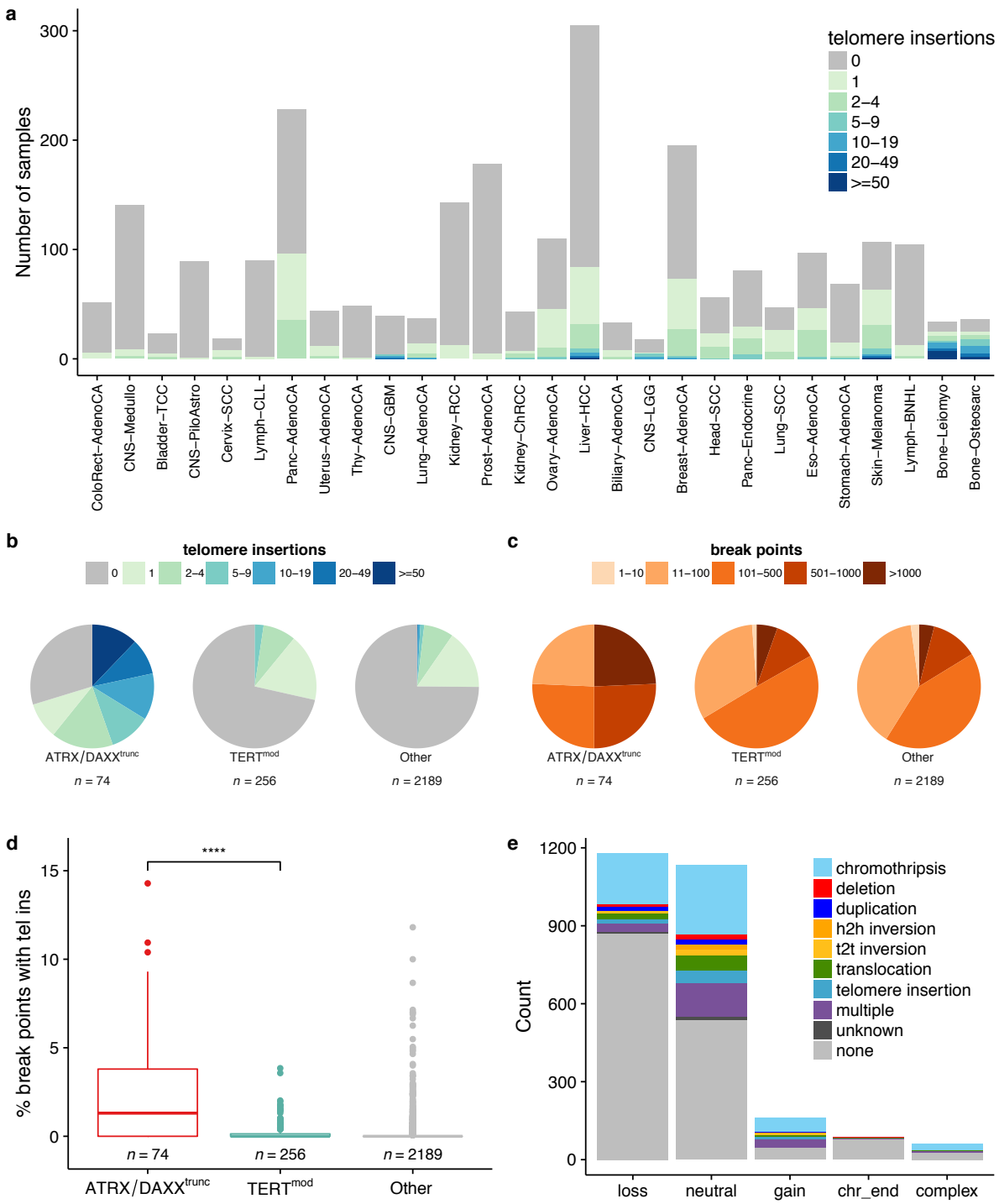

Figure 3: Insertion of telomere sequences into non-telomeric chromosomal regions. (a) Number of telomere insertions in samples of different tumor types. The tumor types are sorted by mean telomere content tumor/control log2 ratios. Cohorts with sample sizes below 15 are not shown. (b) Number of telomere insertions in samples with different TMM-associated mutations. (c) Number of break points in samples with different TMM-associated mutations. (d) Percent of break points coinciding with telomere insertions in samples with different TMM-associated mutations. ****$p < 0.0001$, Wilcoxon rank-sum test. (e) Copy number changes of adjacent segments accompanying telomere insertions. "Complex" means that the copy numbers between segments differ in more than four copies. Overlaps with regions of chromothripsis are indicated. For telomere insertions that did not overlap with regions of chromothripsis, structural variations or additional telomere insertions within 10 kb are indicated. h2h = head-to-head, t2t = tail-to-tail.

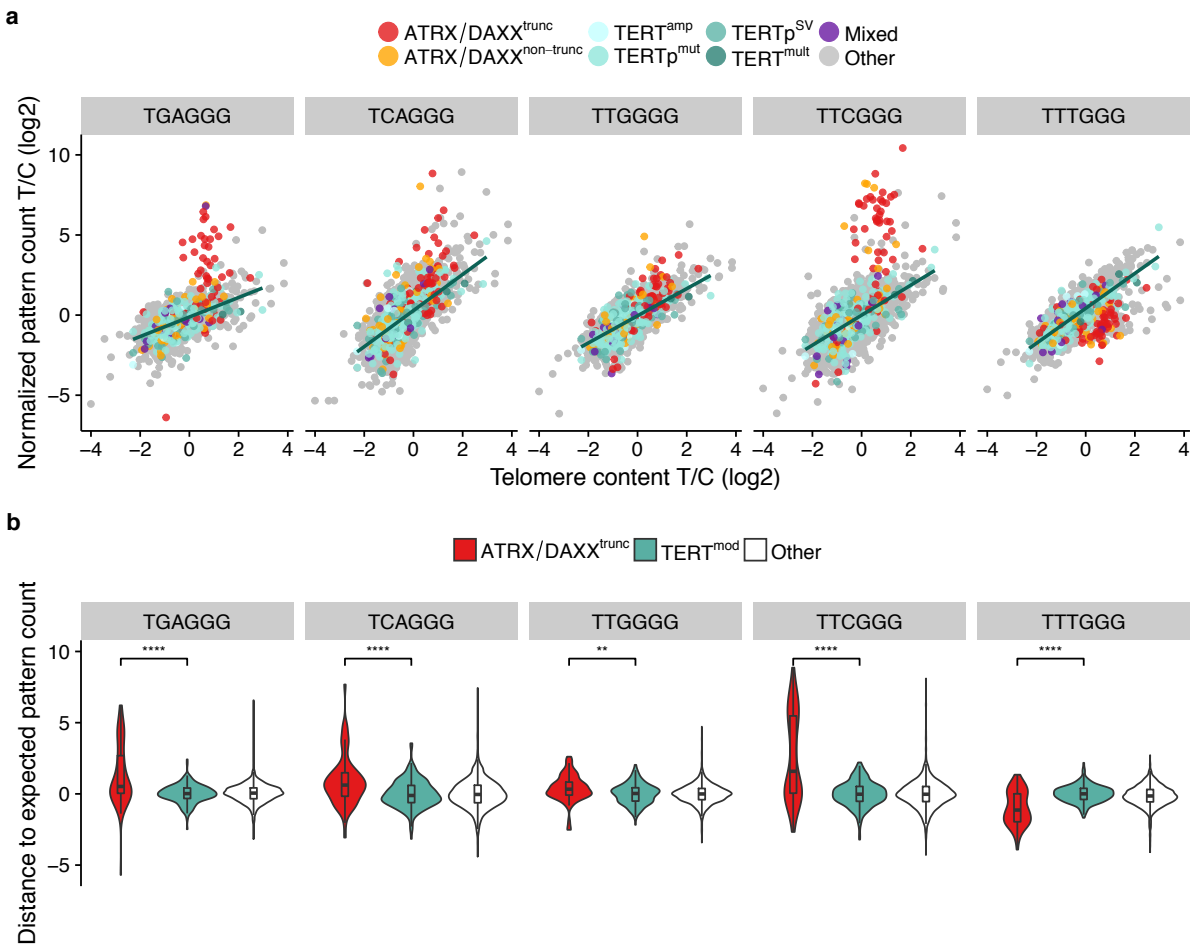

Figure 4: Singleton TVRs enriched or depleted in ATRX/DAXX^{trunc} samples. (a) Pattern count tumor/control log2 ratios of all patients plotted against telomere content tumor/control log2 ratios for selected singleton repeats ((TTAGGG)$_3$-NNNGGG-(TTAGGG)$_3$). The regression line through the TERT^{mod} samples is shown in green and is defined as the expected pattern count in the following. (b) Distance to the expected singleton repeat count in ATRX/DAXX^{trunc} and TERT^{mod} samples. ****$p < 0.0001$; **$p < 0.01$, Wilcoxon rank-sum tests after Bonferroni correction. The profiles of all analyzed patterns are shown in Supplementary Figure 10.

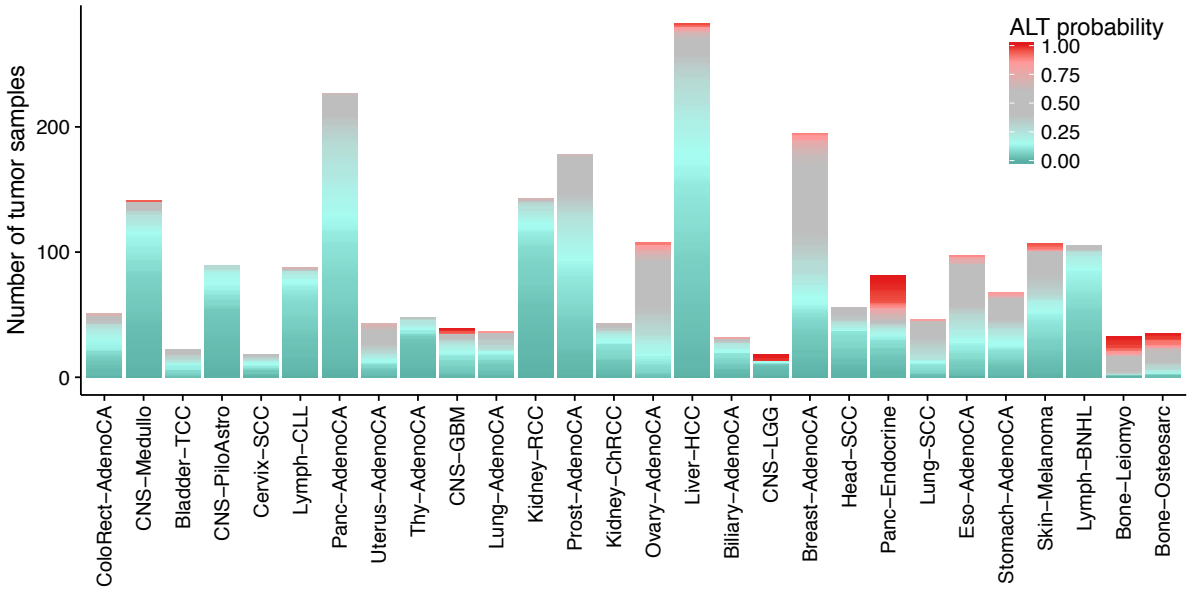

Figure 5: Prediction of ALT probability. For each tumor sample, the ALT probability predicted by a random forest classifier is shown. The tumor types are ordered by mean telomere content tumor/control log2 ratio (from left to right). Cohorts with sample sizes below 15 are not shown.

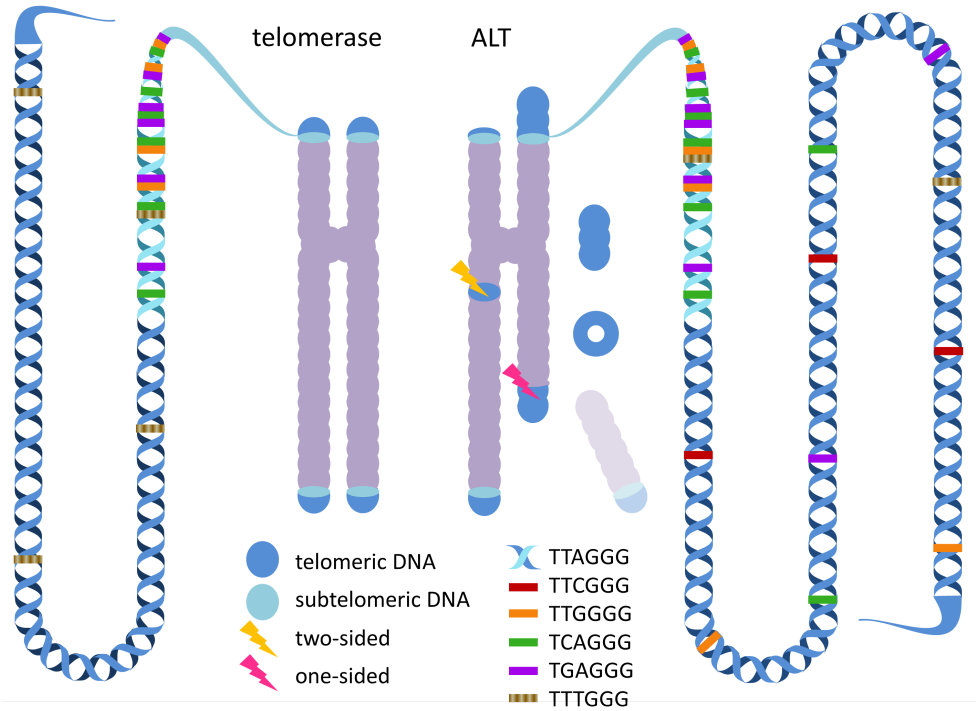

Figure 6: Genomic footprints of telomerase-mediated telomere elongation and ALT.
It is known that telomeres elongated by telomerase have a homologous length with few TVRs in distal telomeric regions (left), while ALT telomeres have heterogeneous lengths with an increased amount of TVRs (right). Moreover, ALT cells have abundant extrachromosomal telomeric sequences. From this study, we conclude that the chromosomes of ALT cells have a higher number of aberrant interstitial telomere insertions, most of which are one-sided and accompanied by a loss of the adjacent chromosomal segment. We also showed that several TVRs occurring as singletons are more abundant in ALT telomeres, while one singleton (TTTGGG) was more abundant in telomerase-elongated telomeres. Please note that it is currently undetermined whether the different types of singletons are located in proximal or distal telomeric regions.

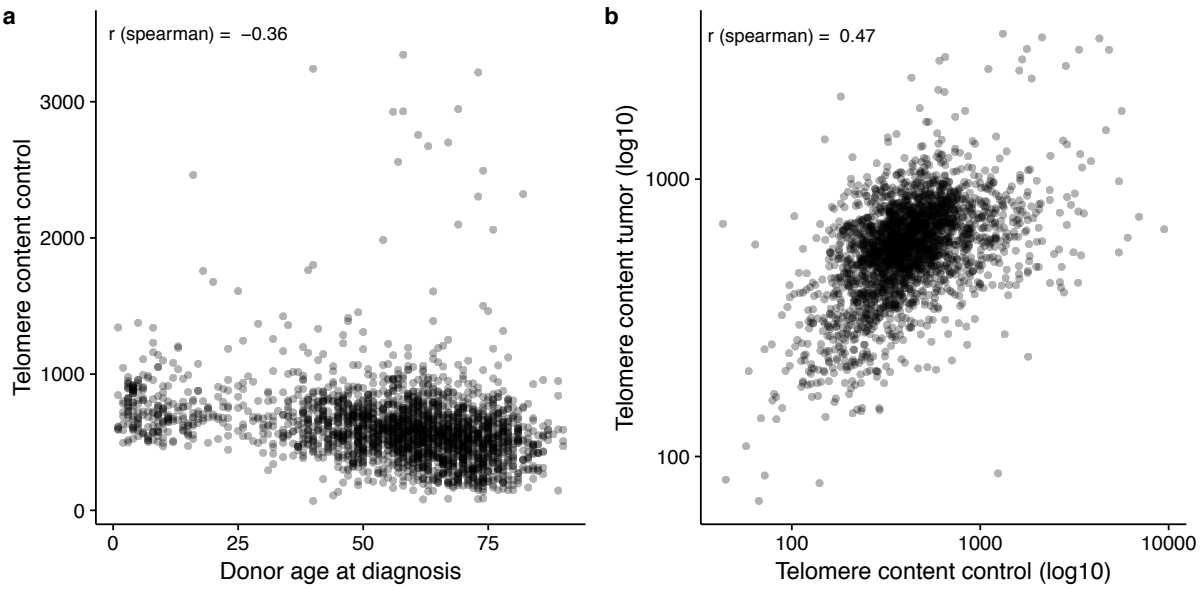

Supplementary Figure 1: Influences on telomere content. (a) Correlation of control telomere content and the patient age at diagnosis. (b) Correlation of telomere content in the tumor and the control sample.

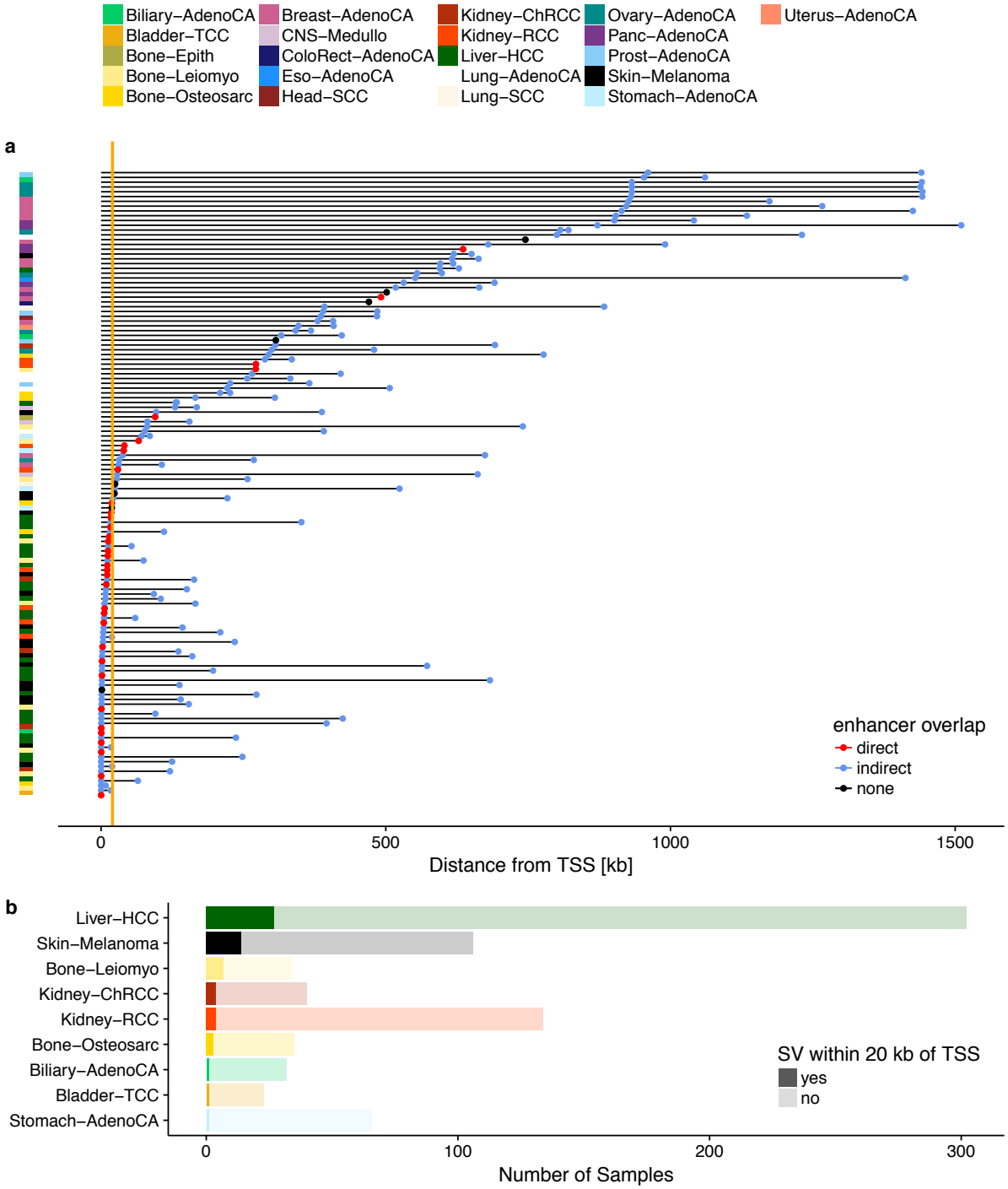

Supplementary Figure 2: Structural variations upstream of *TERT*. (a) Distance of structural variations (SVs) up to 1 mb upstream of the *TERT* transcription start site (TSS). For each tumor sample, only the SV closest to the TSS is shown. Direct overlaps of juxtaposed positions with dbSUPER enhancer regions are indicated in red. dbSUPER enhancers upstream of the SV are shown in blue, where the first point of each line is the position of the SV and the second point is the rearranged enhancer position. All tumor samples with SVs within 20 kb of the *TERT* TSS (orange line) were considered as $TERT^{mod}$ for the further analysis. (b) Number of samples per tumor type with and without an SV within 20 kb of the *TERT* TSS. Only tumor types with at least one affected sample are shown.

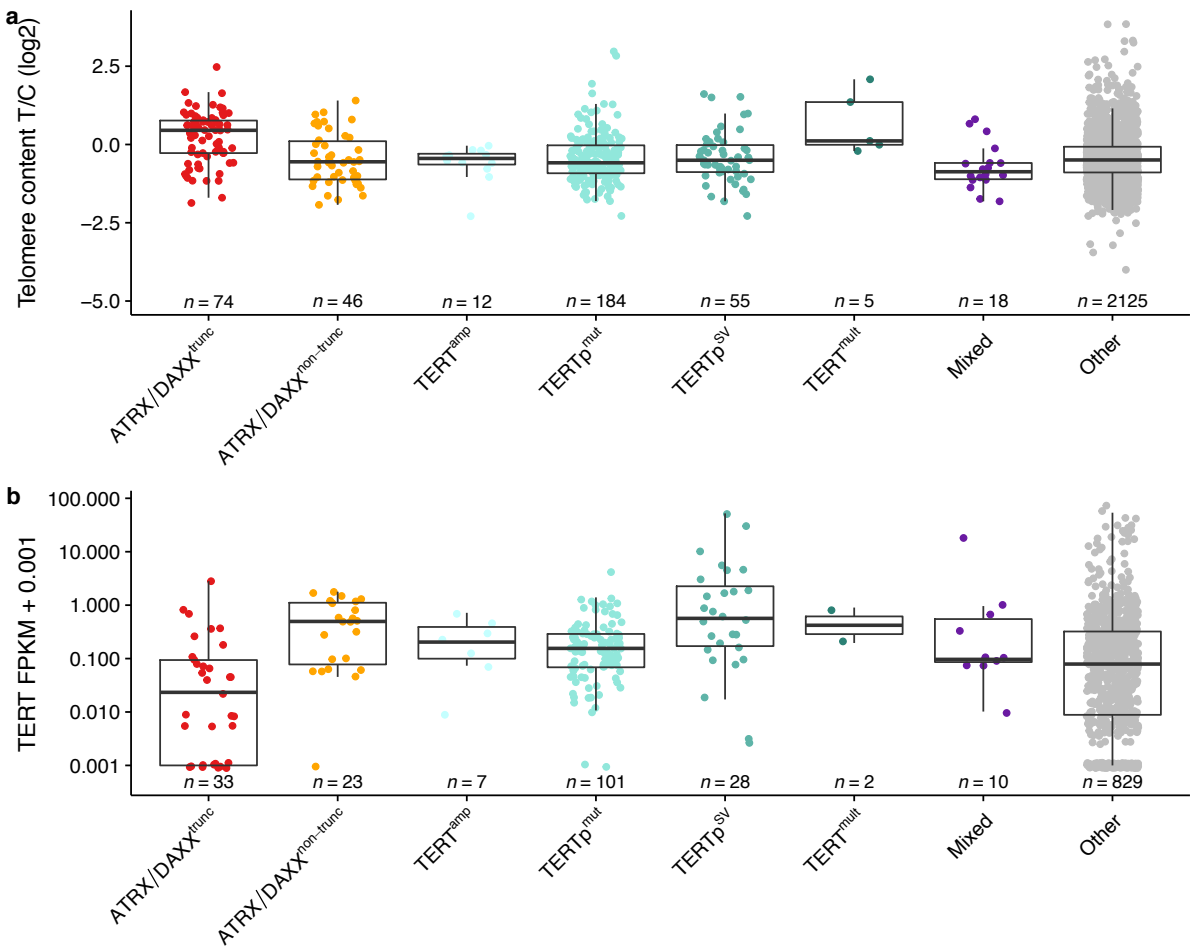

Supplementary Figure 3: Telomere content and *TERT* expression of tumor samples with different TMM-associated mutations. (a) Telomere content tumor/control log2 ratios. (b) *TERT* expression in FPKMs.

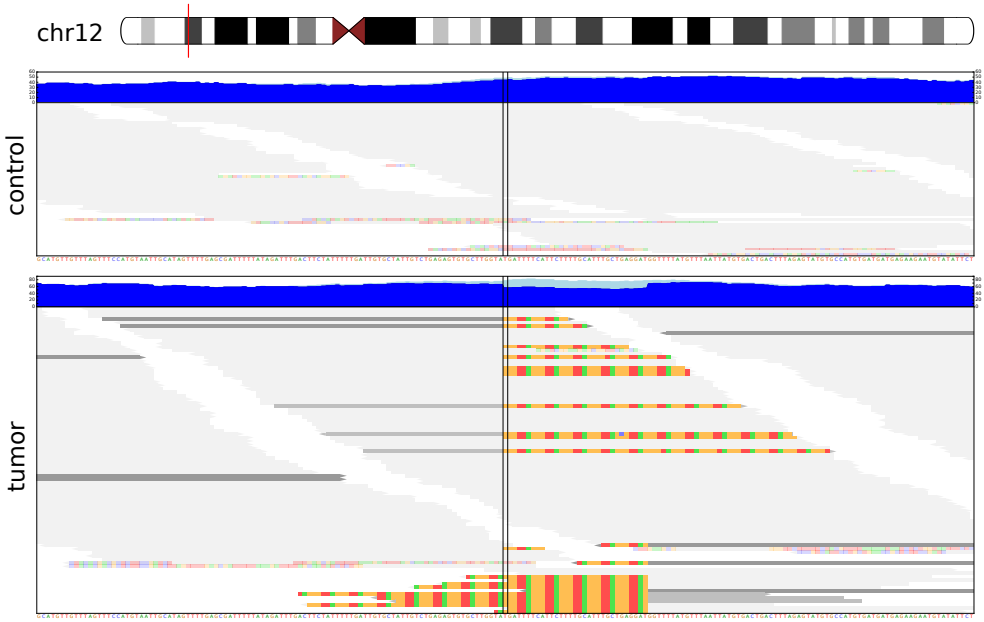

Supplementary Figure 4: Example of reads mapping to a two-sided telomere insertion in breast cancer sample 0a2a3529-f645-4967-9a58-89ee20b8bb62. See Figure 2 for a detailed description.

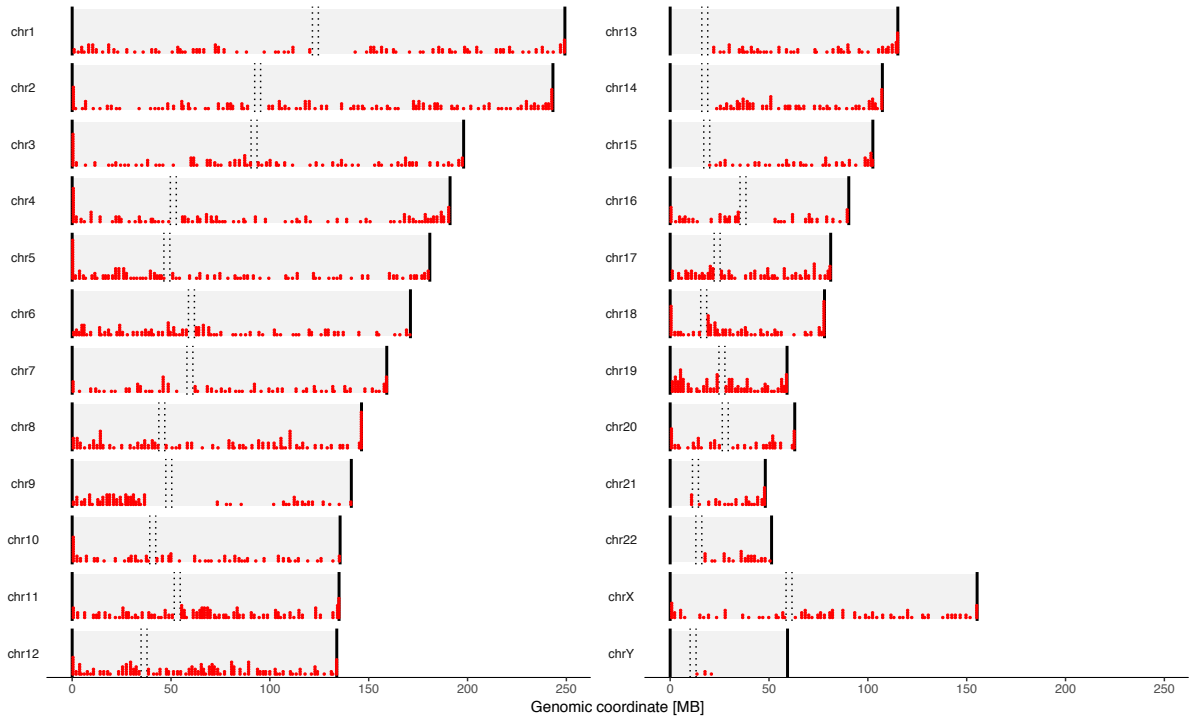

Supplementary Figure 5: Chromosomal positions of telomere insertions.

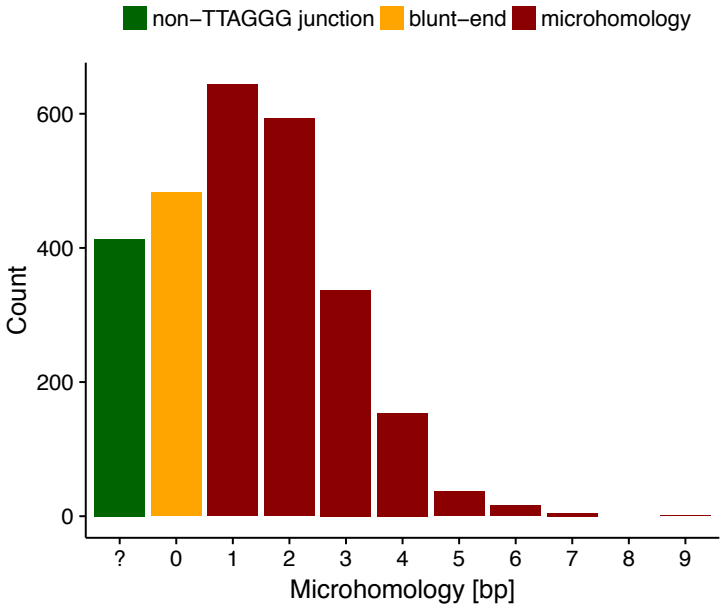

Supplementary Figure 6: Patterns of microhomology at telomere insertions. The number of homologous bases between the canonical TTAGGG telomere repeat and the human reference genome at telomere insertions is shown on the x-axis. The number of telomere insertions with a pattern of TTAGGG microhomology (red), blunt-end DNA joining (yellow) or without TTAGGG repeats at the junction site (green) are shown on the y-axis.

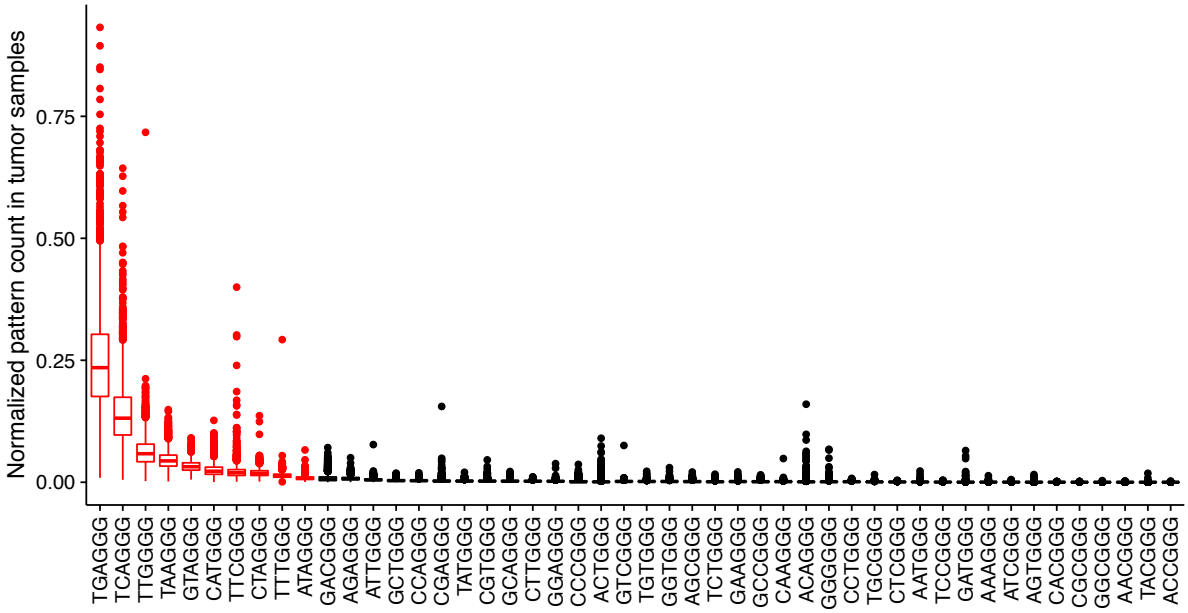

Supplementary Figure 7: Frequency of TVRs in arbitrary context. The mean pattern counts per telomere read are shown for all tumor samples. TVRs shown in red were investigated further regarding sequence context.

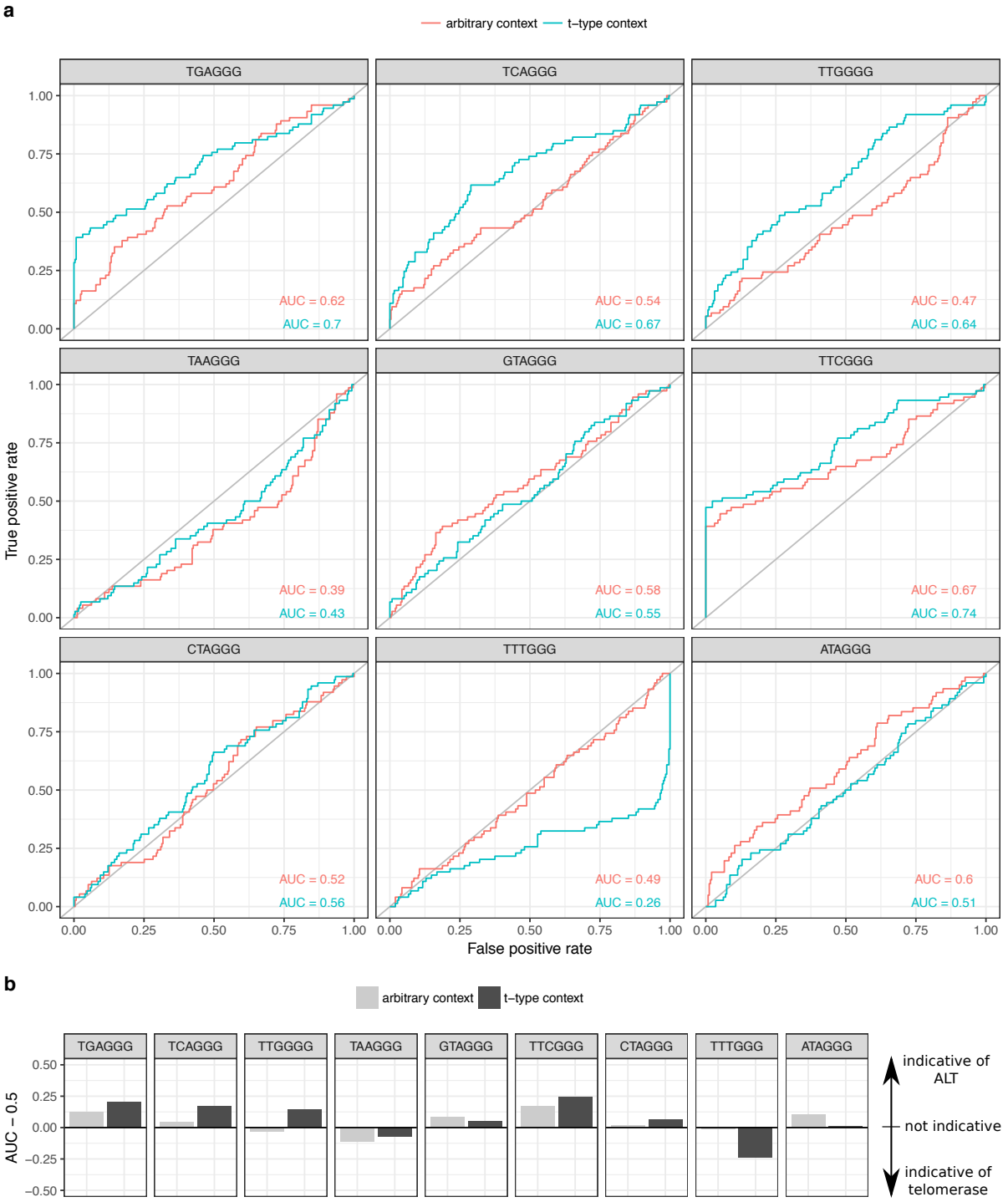

Supplementary Figure 8: The neighborhood of TVRs is indicative of the telomere maintenance mechanism. (a) Receiver operating characteristic for the classification of samples with ALT-associated mutations from telomere repeat variants. Red: no specific sequence context required. Blue: singleton repeats ($(TTAGGG)_3$-NNNGGG-$(TTAGGG)_3$). (b) Area under the curve (AUC) for the classification of ALT using repeat type counts in different sequence context.

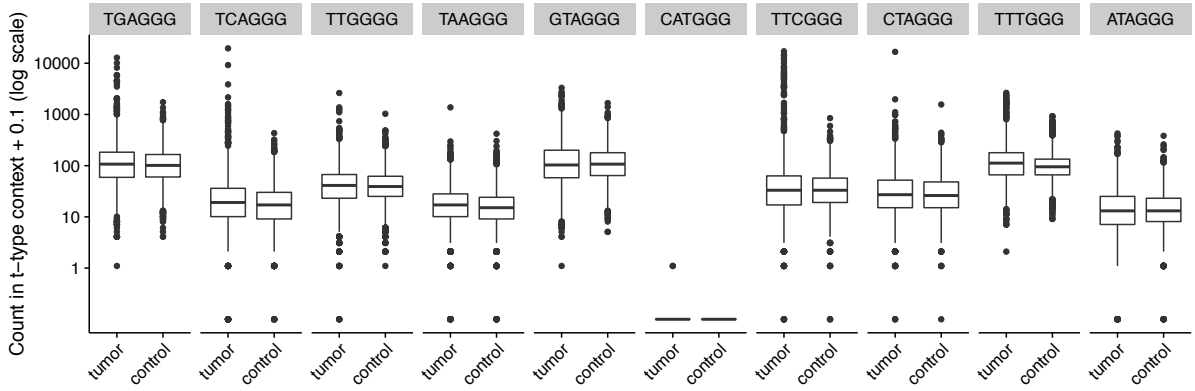

Supplementary Figure 9: Raw counts of singleton TVRs across all samples.

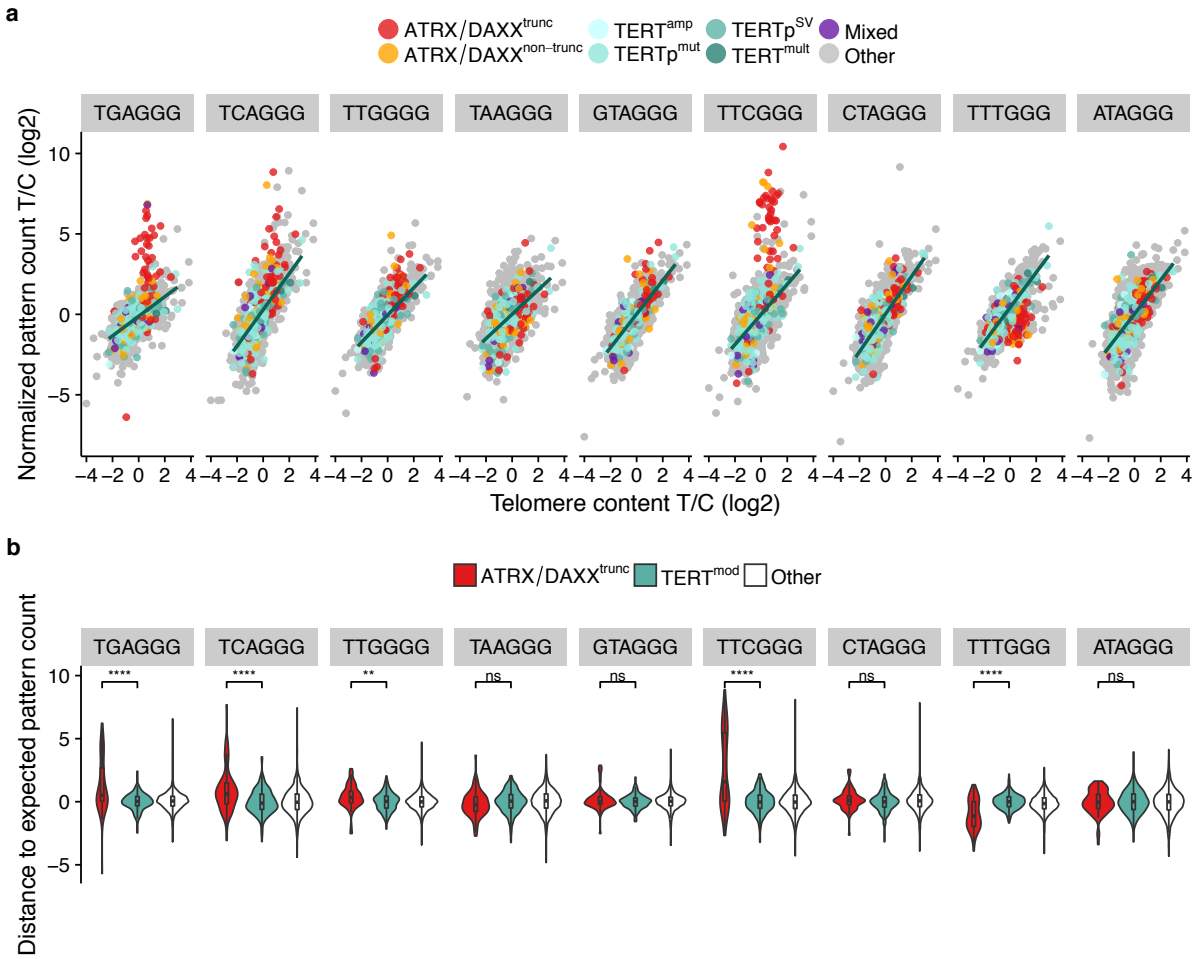

Supplementary Figure 10: Singleton TVRs. See Figure 4 for details.

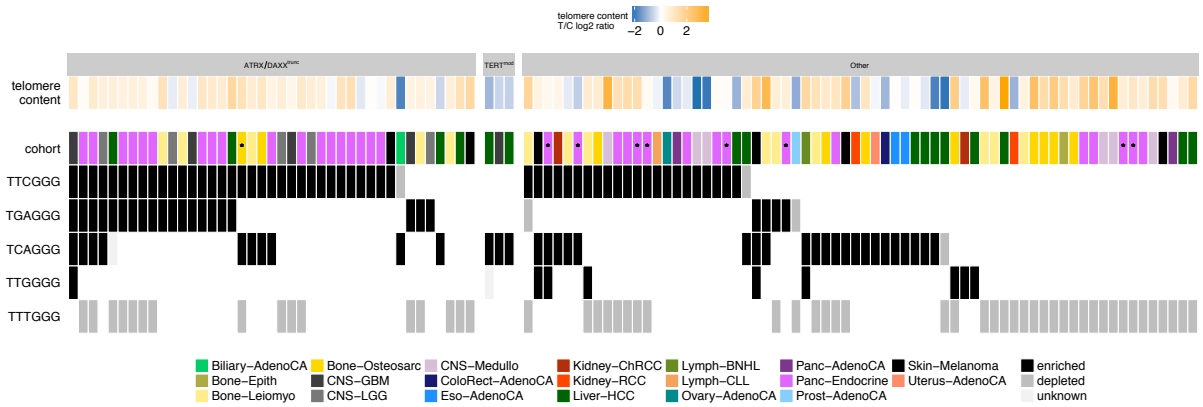

Supplementary Figure 11: Co-occurrence of singleton TVRs. Each column represents a patient. Enrichment is defined as a distance to the expected patterns occurrence larger than 2.5. Depletion is defined as a distance smaller than -2. Asterisks in the cohort row indicate non-truncating mutations in *ATRX* or *DAXX* that are non-synonymous point mutations, stop-codon losses or point mutations at splice sites.

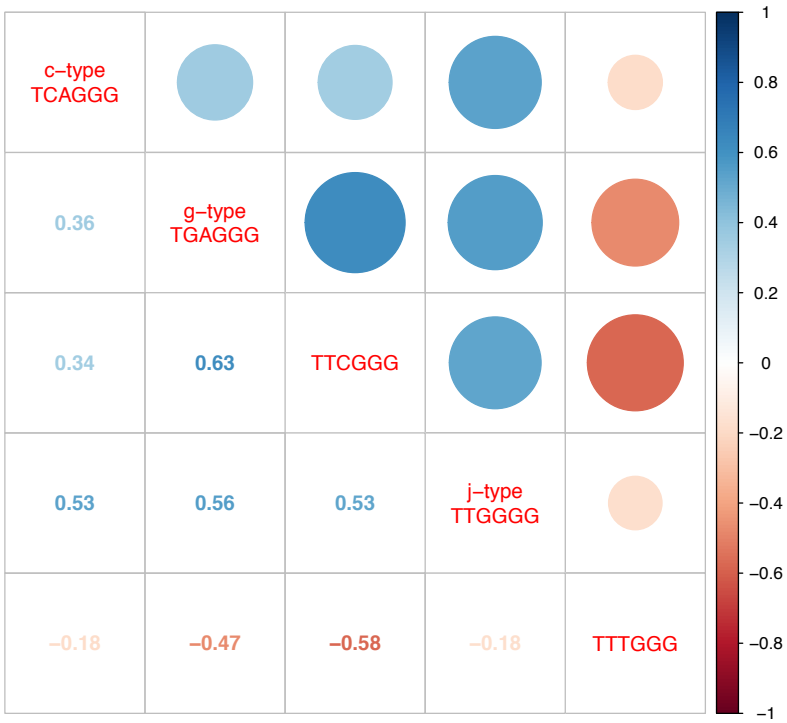

Supplementary Figure 12: Correlation of singleton TVRs in ATRX/DAXX^{trunc} samples. The Pearson correlation coefficients for the occurrence of the significantly enriched/depleted singleton TVRs in ATRX/DAXX^{trunc} samples is shown.

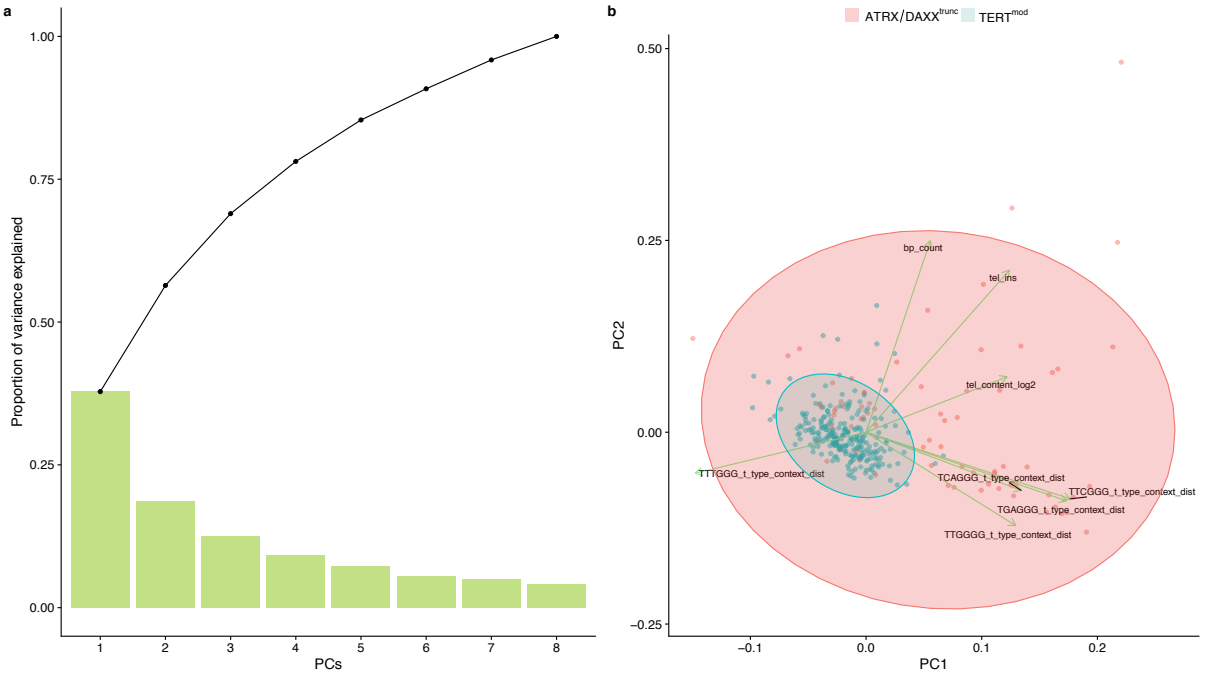

Supplementary Figure 13: Principal component analysis. The features used for the analysis were: telomere content tumor/control log2 ratio, number of telomere insertions, number of break points and the distance of TGAGGG, TCAGGG, TTGGGG, TTCGGG and TTTGGG singleton repeats to their expected occurrence. (a) Proportion of variance explained by different principal components (green bars). The black line shows the cumulative variance explained. (b) Features distinguishing ATRX/DAXX^{trunc} and TERT^{mod} samples with ALT-associated and telomerase-associated mutations mapped onto the first two principal components (PCs). All 327 samples used for the analysis are plotted on the first and second PCs.

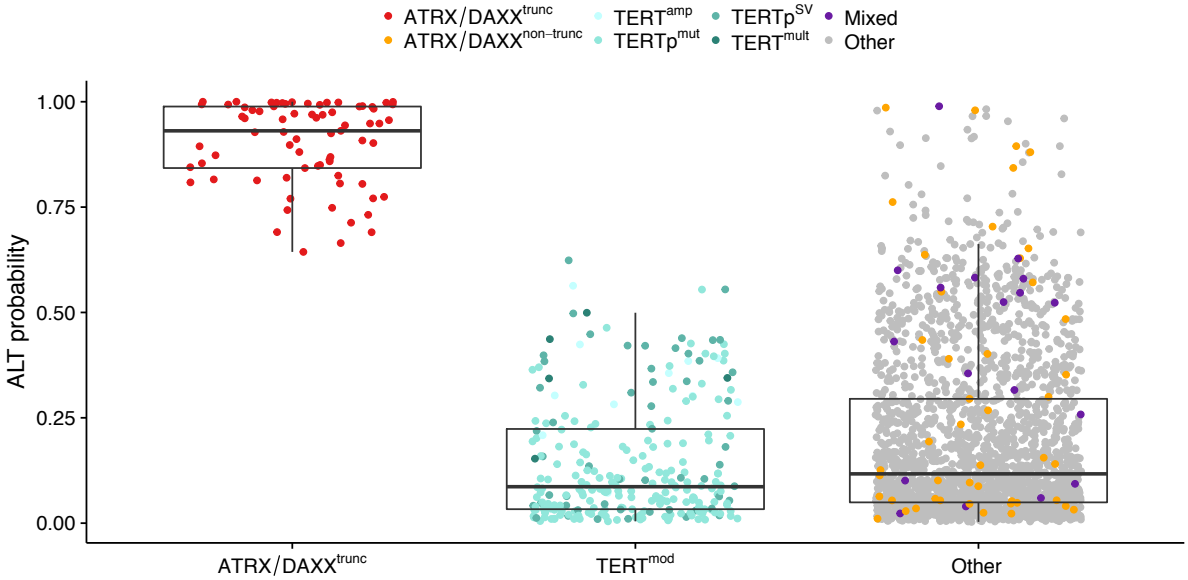

Supplementary Figure 14: ALT probability of tumor samples with different TMM-associated mutations. The ALT probability was derived from a random forest classifier trained to distinguish ATRX/DAXX^{trunc} from TERT^{mod} samples based on the following features: telomere content tumor/control log2 ratio, number of telomere insertions, number of break points and the distance of TGAGGG, TCAGGG, TTGGGG, TTCGGG and TTTGGG singleton repeats to their expected occurrence.